Scientific Research Publishing

International Journal of Geosciences, 2025, 16(4), 204-223
https://www.scirp.org/journal/ijg
ISSN Online: 2156-8367
ISSN Print: 2156-8359

New Lithological, Petrographic and Geochemical Data from the Karthala Lava Massif, Grande Comore, Indian Ocean

Adinane Ahamada[1*], Samba Cissokho[1], Ibrahima Labou[2], Mahamadane Diene[2], Ali Rachidi Oikifou[1], Papa Malick Ngom[1]

[1]Department of Geology, Faculty of Sciences and Technics, Cheikh Anta Diop University, Dakar, Senegal
[2]National Superior School of Mines and Geology, Cheikh Anta Diop University, Dakar, Senegal
Email: *adinane.ahamada@ucad.edu.sn

How to cite this paper: Ahamada, A., Cissokho, S., Labou, I., Diene, M., Oikifou, A.R. and Ngom, P.M. (2025) New Lithological, Petrographic and Geochemical Data from the Karthala Lava Massif, Grande Comore, Indian Ocean. *International Journal of Geosciences*, **16**, 204-223.
https://doi.org/10.4236/ijg.2025.164011

Received: March 2, 2025
Accepted: April 14, 2025
Published: April 17, 2025

Abstract

The Karthala massif, which covers the entire central and southern part of the island of Grande Comore, is made up of massive basalt flows, both vesicular and non-vesicular, pahoehoe and aa-type lavas and oceanite boulders. Petrographic observations of massive basalt flows show porphyritic and vacuolar microlitic textures marked by successive crystallization of opaque minerals, olivines, clinopyroxenes, orthopyroxenes and plagioclases in little or no mesostasis. This crystallization sequence is characteristic of a high-pressure geodynamic environment. The chemical variation of major and trace elements shows that the basalts studied are characterized by an under-saturation in silica (47.44%) and an enrichment in alkalis (1.95%) and titanium (2.33%). The rare-earth spectra of these basalts show a subparallel pattern, suggesting the same source. In the rare earth and multi-element diagram, the Karthala basalts show an alkaline nature, characterized by enrichment in light rare earths (LREE) and large ion lithophile elements (LILE) and depletion in heavy rare earths (HREE) and high field strength elements (HFSE). They also show positive Nb and Ta anomalies, typical of oceanic island basalts (OIBs) emplaced by mantle plume dynamics. These geochemical characteristics are compatible with an enriched, deep-seated garnet lherzolite-type source.

Keywords

Grande Comore, Karthala Massif, Mantle Plume, Hot Spot, Oceanic Island Basalts

1. Introduction

The Karthala massif on the island of Grande Comore is an active volcano whose origin, nature of source and geodynamic context of rock emplacement remain subjects of debate. In this context, the authors [1]-[5] suggest a mantle source of the hot-spot type, attributing the volcanism of the Comoros to a mantle plume and emphasizing the interaction between the lithosphere and the fluids of this plume. [6] interpret the Comoros volcano as a hot spot located on an intraplate fracture zone, a passive margin, or the northern limit of a zone of diffuse deformation. In contrast, [6] and [7] question the contribution of a hot-spot and propose in this case the presence of lithospheric fracture. [8] support the idea of lithospheric deformation in the context of the East African Rift. Controversy persists as to the crustal nature of the Comoros Basin, based on petrological and magnetic studies. Indeed, [9] and [10] and, suggest that the Mozambique Channel between Africa and Madagascar constitutes a geosyncline resting on a Precambrian granitic ridge. [10] and [11] support this hypothesis on the basis of sandstone enclaves in the lavas of the Comoros Islands. However, [12] identified magnetic anomalies in the western Somali basin, suggesting that the crust of this basin is oceanic.

This simple bibliographical review shows the importance of this study, whose aim is to provide new lithological, petrographic and geochemical data for a better understanding of the geology of the Karthala massif, to better elucidate the nature and depth of the magmatic source and to propose a geodynamic scenario for the emplacement of the rocks.

2. Geological Context

2.1. Regional Geological Context

The Comoros archipelago is located in the Indian Ocean, more precisely in the Mozambique Channel, halfway between Madagascar and Africa [10]. From north to south and west to east, it comprises four (04) islands (**Figure 1**): Grande Comore; Mohéli; Anjouan and Mayotte (**Figure 1**).

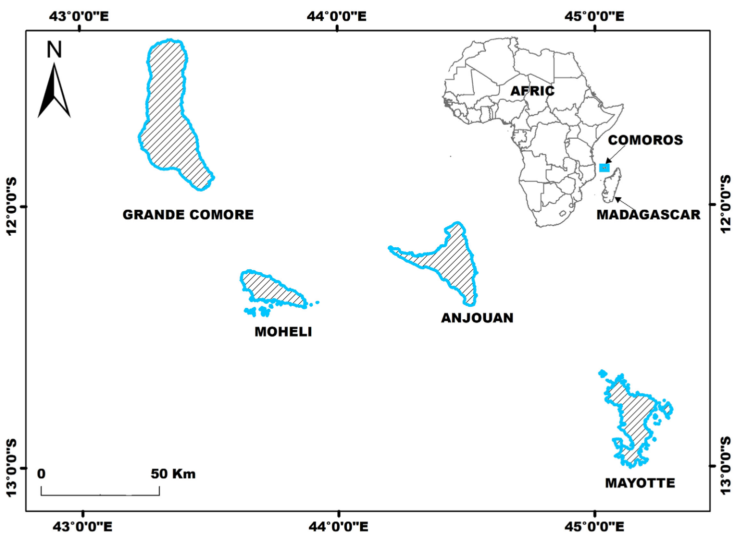

Figure 1. Location map of the comoros archipelago [10], modified.

The Comoros archipelago was formed in the Cenozoic, following the detachment of Africa in the Lower Jurassic [13]. These islands were formed as a result of age-dependent progressive volcanism from the ESE to the WNW of the archipelago [3] [7] [14]. These authors deduce that the oldest volcanism began in the Cretaceous-Miocene, after volcanism had migrated westwards to form the four islands. Thus, Maoré (Mayotte) existed in the Mio-Pliocene, Anjouan and Mohéli in the Pliocene [13] and Grande Comore or Ngazidja in the Quaternary [13].

The Mozambique Channel, which lies between the relatively steep and narrow continental slopes of the African continent and the island of Madagascar, began its formation during the break-up of Gondwana and continues to the actual [10] and [15]:

- The movement of Madagascar in relation to Africa, which was guided by a dextral transform fault of submarine relief: the Davie Range [12].
- The Davie Range (2000 km wide) illustrates the movement between Madagascar and Africa from the Middle-Upper Jurassic to the Aptian [16].
- The separation of Madagascar from east Africa is associated with the opening of the Somali and Mozambique basins by N-S oceanic accretion along the mid-ocean ridge [17].

2.2. Local Geological Context

The island of Grande Comore has been subdivided into three (03) massifs based on geomorphological considerations [18]: Grille in the north, Karthala in the center and Badjini in the extreme south (**Figure 2**).

However, it should be noted that Grande Comore is made up of two (02) large shield volcanoes: the Grill massif to the north and the Karthala massif (the center and south of the island) [19]. The latter, the site of our study area, is a large active volcano with a poly-lobed summit caldera whose morphology is marked by the presence of two craters: the Chungmu Chahalé crater in the center and the Chagnoumeni crater in the north, a few hundred metres from the Itsandra gate. Major volcanic eruptions have produced lava flows that have emerged either from the summit crater or, more often, from lateral fissures marked by a large number of small adventitious strombolian cones [13].

The formations of the Karthala massif have been subdivided by [18] into three (03) volcanic units according to the presence or absence of surface flow structures (see **Figure 3** below).

- A first unit corresponding to the ancient Karthala (K5 and K6), which corresponds to the ancient Badjini massif. This unit is highly altered, lacking any flow surface structure, and develops layers of ferralitic alterites of decimetric to metric thickness;
- A second unit characterized by little altered formations constituting the recent Karthala (K4a and K4b), formed of pahoehoe and aa-type flows, aphyric basalts and olivine megacrysts;
- And a third unit made up of the younger formations that make up actual

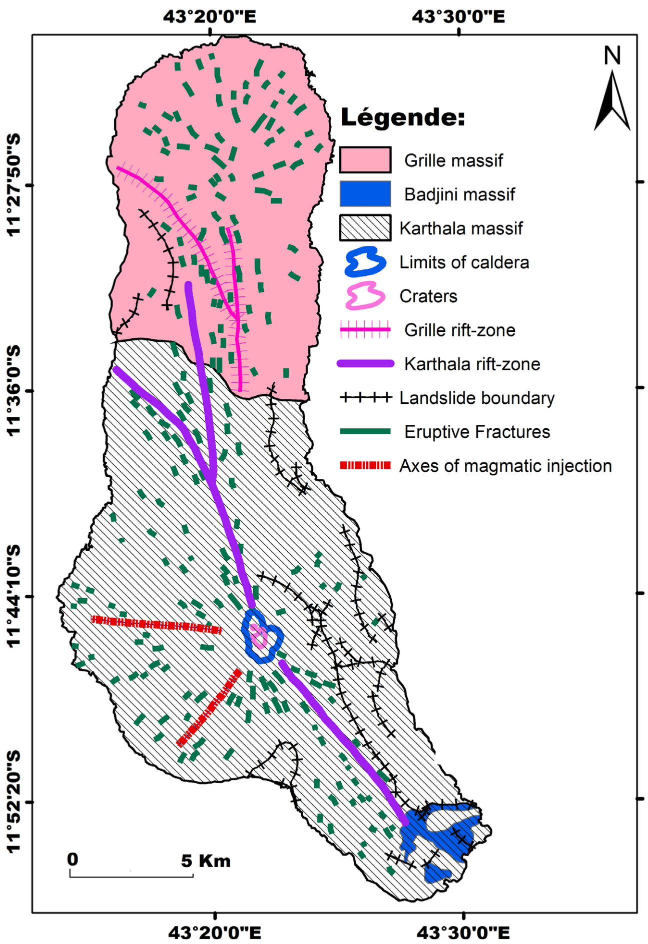

Figure 2. Geomorphological map of Grande Comore [18], modified.

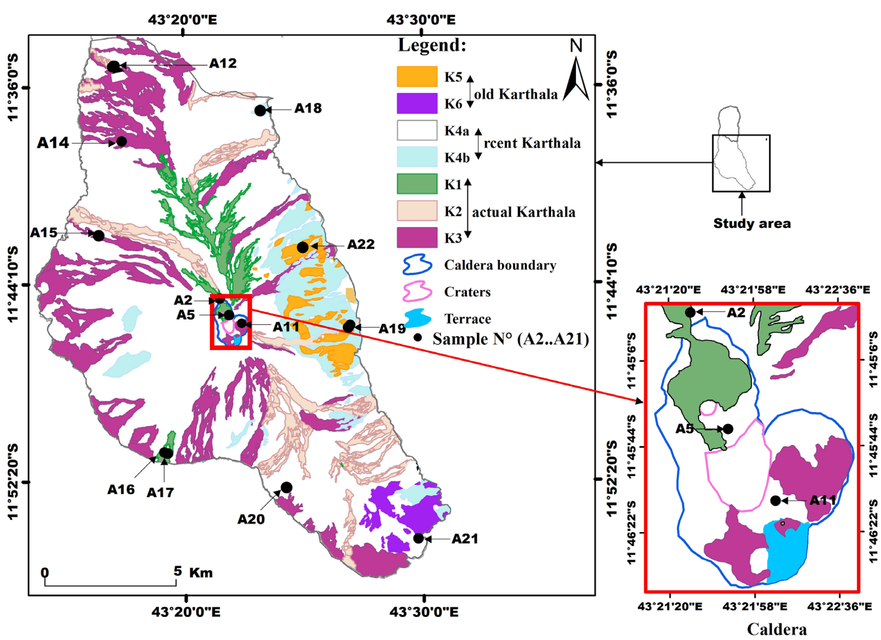

Figure 3. Volcano-tectonic map of the Karthala massif [18], modified, showing the location of sampling points.

Karthala (K1, K2 and K3), devoid of vegetation and with the marked surface characteristics of well-preserved flows.

3. Methodology

The methodology used throughout this work consisted firstly of fieldwork based on the identification of the various lithologies and systematic sampling of the different volcanic facies of the Karthala massif. Following this fieldwork, nineteen (19) rock samples were collected, thirteen (13) of which were selected for geochemical analysis. Of these samples, ten (10) are basalts, one (1) is an ankaramite and two (2) are oceanites.

After sampling, the thin sections required for petrological studies were prepared at the thin section laboratory of the Houphouët-Boigny University in Ivory Coast. Petrographic studies were then carried out using a camera-equipped optical microscope at the Geology Department, the National Superior School of Mines and Geology (ENSMG) and the Fundamental Institute of Black Africa (IFAN) of the Cheikh Anta Diop University of Dakar (UCAD). Finally, geochemical analyses of total rock (major and trace elements) were carried out in Canada by the ACTLABS laboratory. Major elements were analyzed by the FUS-ICP method and trace elements by the FUS-ICP and FUS-MS methods.

4. Results

4.1. Lithological and Petrographic Studies

Lithological and petrographic studies were carried out mainly on the three volcanic units of the Karthala massif (ancient, recent and actual), the sampling points of which are located on the volcanotectonic map of Grande Comore (**Figure 3**).

The lithological study shows that the Karthala massif is characterized by an eruptive dynamism that gives rise to flows of different shapes divided into three units:

- First unit: porphyritic vesicular basalt flows;
- The second unit is made up of non-vesicular porphyritic basalt flows, ankaramites and pahoehoe-type flows;
- And third unit made up of porphyritic vesicular basalt flows, oceanites and aa-type flows.

Porphyritic vesicular basalts have been subdivided into two types according to the abundance and nature of the phenocrysts: vesicular basalts with clinopyroxene and orthopyroxene phenocrysts and vesicular basalts with olivine phenocrysts.

- Clinopyroxene and orthopyroxene phenocrystalline vesicular basalts outcrop at the Karthala summit at the northern entrance to Itsandra gate, 1.18 km from the large Chungu Chahalé crater. The rocks are heaped into angular blocks of decimetric to metric size, showing a light-grey hue in fresh fracture. It should be noted, however, that these porphyritic basalts look aphyritic at the outcrop scale (**Figure 4(a)**).
- Vesicular basalts with abundant phenocrysts of olivine and clinopyroxenes

(**Figure 4(b)**), on the other hand, outcrop to the southeast in the Singani sector, 9.36 km from the caldera, and to the northwest in the village of Hasseindjé. They cut into isolated, blunt, polygonal blocks and appear as compact, blackish-grey rocks.

Microscopically, both types of basalt show the same vacuolated porphyritic microlitic texture, composed of plagioclases, clinopyroxenes, orthopyroxenes or olivines as the case may be, opaque minerals and vesicles bathed in little or no mesostasis (**Figure 4(c)** and **Figure 4(d)**).

Plagioclases are very abundant (55% to 65%) and occur as microlites.

Clinopyroxenes (30% to 35%), sometimes macerated, occur as automorphic to subautomorphic phenocrysts (0.4 to 1.2 mm) and small crystals.

Orthopyroxenes are rarely found (1% to 2%) as automorphic to subautomorphic phenocrysts (0.3 to 1 mm), only associated with clinopyroxene phenocrysts.

Olivines (10% to 15%) occur as automorphic to subautomorphic phenocrysts (0.6 to 1.3 mm). Some individuals contain opaque mineral crystals.

The vesicles (3% to 6%) are generally rounded to subrounded and show no filling. Their walls are lined with plagioclase microlites.

Non-vesicular porphyritic basalts (**Figure 4(e)**) outcrop to the northwest of the Karthala massif, around 6 km from the Bangaani sector and 13.8 km from the Karthala summit. These basalts have a very limited thickness (20 m). Microscopically, the rock shows a porphyritic microlitic texture with phenocrysts of clinopyroxenes and olivines containing crystals of opaque minerals (2% - 5%) and a mesostasis containing micolites of plagioclase (60% - 65%) and clinopyroxenes (**Figure 4(f)**).

Oceanites occur mainly in the vicinity of the large Chahalé crater, in the form of scattered light-gray decimetric to millimetric blocks with abundant olivine phenocrysts (**Figure 4(g)**). They are embedded in a platform composed of heterogeneous elements (volcanic ash, black sand, slag and lapillis) from the Karthala volcanic eruptions. Microscopically, the rock shows a porphyritic microlitic texture composed of olivine phenocrysts (30% - 35%) and clinopyroxenes (5% - 7%), and a mesostasis composed of plagioclase microlites (55% - 60%), clinopyroxenes and opaque minerals (**Figure 4(h)**).

Ankaramites outcrop in the Ourovéni area in the extreme south of Grande Comore, 19.7 km from the Karthala volcano, in the form of massive centimetric to metric vesicular blocks. Petrographically, ankaramites have the same texture and mineralogical composition as oceanites, but are distinguished from the latter by the abundance of clinopyroxene phenocrysts (**Figure 4(i)** and **Figure 4(j)**). Some clinopyroxene phenocrysts include olivine crystals (**Figure 4(k)**).

Pahoehoe-type flows or corded lavas appear as pleated rope clusters (**Figure 4(l)**). They are in the form of cow dung, with small folds wound around each other on their surface to form entrainment folds.

Type aa flows have a rough, irregular surface with decimetric to metric sharp blocks colonized by lichens and moss (**Figure 4(m)**). It should be noted, however, that we were unable to make thin slides of the pahoehoe and aa-type flows due to their very brittle nature.

Basalt stalactites formed by dripping lava are very common in the study area (**Figure 4(n)**).

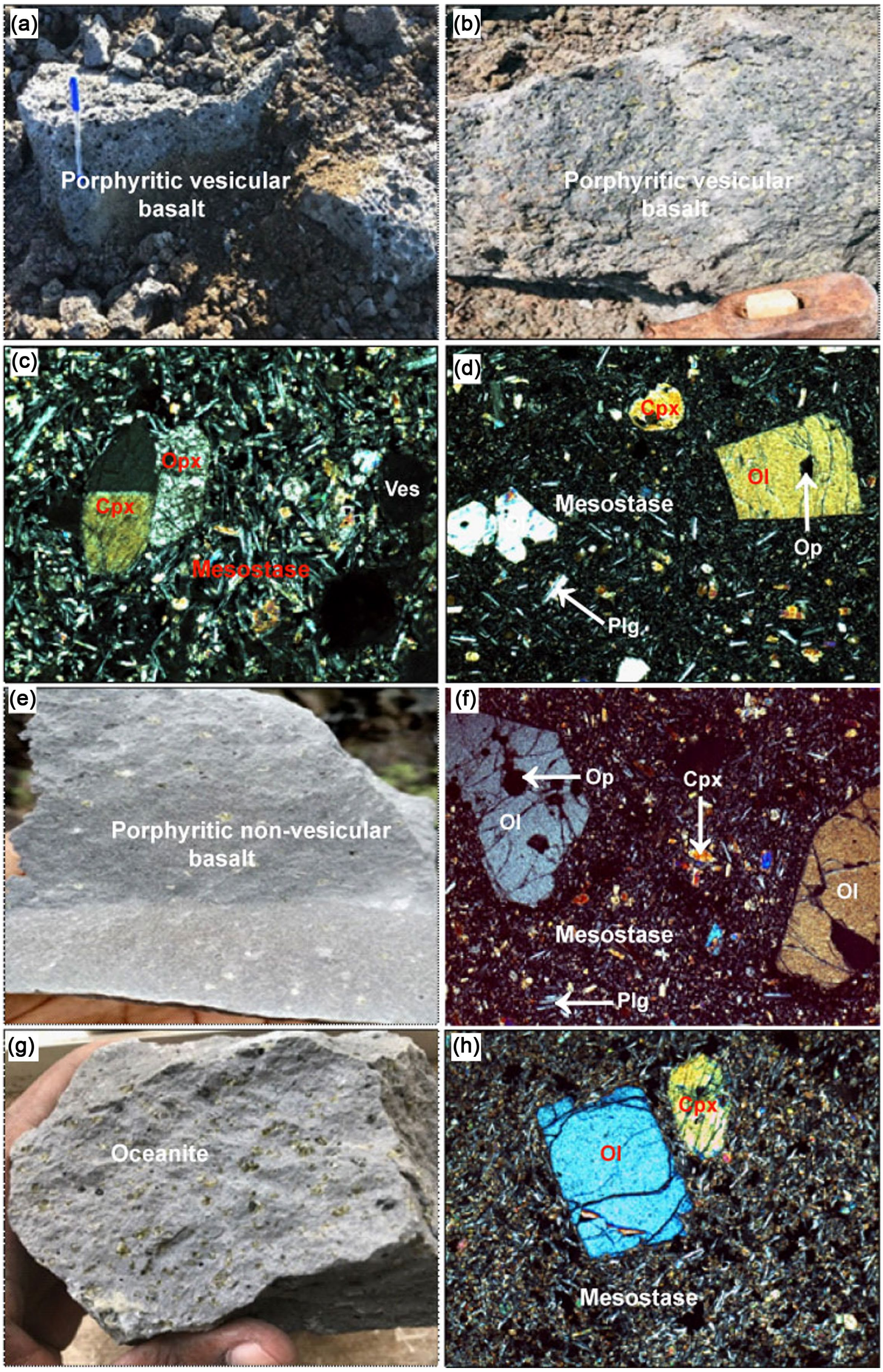

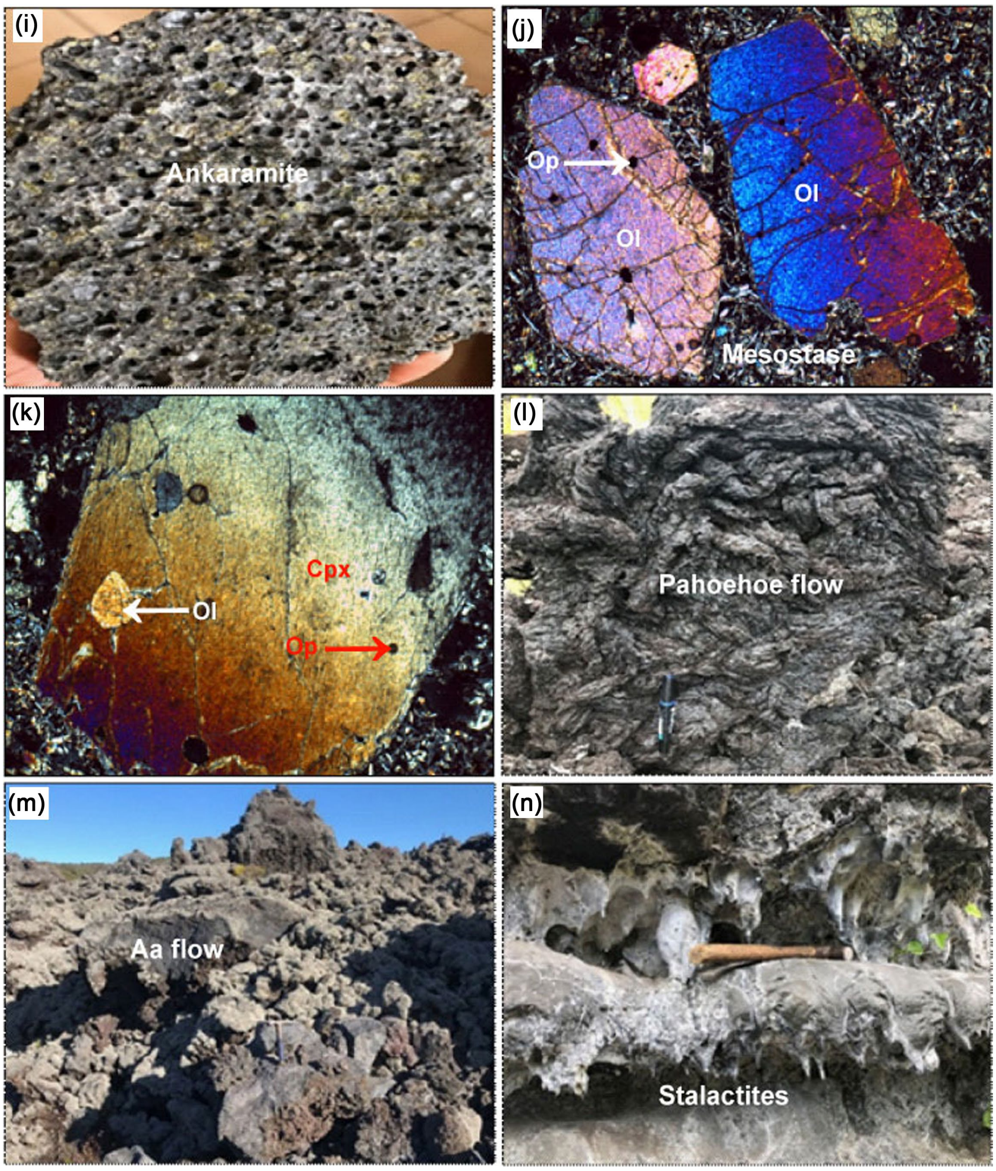

Figure 4. (a) Vesicular basalt showing an aphyric appearance at outcrop scale; (b) porphyritic vesicular basalt showing olivine (Ol) phenocrysts; (c) microscopic characteristics of aphyric vesicular basalt showing clinopyroxene (Cpx) and orthopyroxene (Opx) phenocrysts; (d) microscopic characteristics of porphyritic vesicular basalt showing clinopyroxene and olivine phenocrysts enclosing opaque minerals (Op); (e) and (f) macroscopic and microscopic characteristics of non-vesicular porphyritic basalts showing phenocrysts of olivines enclosing opaque minerals; (g) and (h) macroscopic and microscopic characters of oceanites illustrating a porphyritic microlitic texture with clinopyroxene and olivine phenocrysts bathing in a very abundant mesostasis; (i)-(k) macroscopic and microscopic characters of ankaramite showing clinopyroxene and olivine phenocrysts. Some clinopyroxene phenocrysts include olivine phenocrysts; (l) macroscopic characteristics of Pahoehoe-type flows in the form of folded rope clusters; (m) macroscopic characteristics of aa-type flows showing decimetric to metric sharp blocks colonized by lichens and moss and (n) basalt stalactites formed by lava dripping.

4.2. Geochemical Study

The geochemical study will be carried out according to the three units already identified on the Karthala massif, *i.e.* ancient, recent and actual Karthala. A total of 13 rock samples were selected for geochemical analysis, with concentrations of major and trace elements shown in **Table 1**. Of these samples, 2 belong to ancient Karthala, including 1 porphyritic vesicular basalt and 1 porphyritic non-vesicular basalt, 5 to recent Karthala, including 1 porphyritic vesicular basalt, 1 porphyritic non-vesicular basalt, 1 ankaramite and 2 oceanites, and 6 to actual Karthala, including 4 porphyritic vesicular basalts and 2 porphyritic non-vesicular basalts. It should be noted, however, that all these samples have very low losses on ignition (LOI) ranging from 0.16% to 0.91%, suggesting that chemical elements such as LILE and HFSE are very little affected by post-magmatic phenomena such as metamorphism, hydrothermalism, seawater, tectonics and oxidation. Therefore, the geochemical characters of all rock samples will be examined in this section. In addition, REEs are normalized to the NWA974 chondrites of [20], while incompatible trace elements are normalized to the primitive mantle of [21].

4.2.1. Major and Trace Elements

Plotting the geochemical data of the Karthala massif rocks on the Zr/TiO_2 versus Nb/Y diagrams of [22] and Zr/Ti versus Nb/Y diagram of [22] modified by [23] shows that all samples have an alkaline basalt composition (**Figure 5(a)** and **Figure 5(b)**). However, the ancient Karthala basalts have higher contents of major elements such as SiO_2 (48% - 48.7% vs. 46.4% - 47.9%), TiO_2 (2.6% vs. 1.6% - 2.5%), Na_2O (3.1% vs. 1.8% - 3.1%) and K_2O (1.2 vs. 0.6% - 1.1%) and incompatible trace elements such as Y (25.8% - 26.1% vs. 16.5% - 23.9%) and Yb (2% vs. 1%, 3% - 1.8%) but lower values in Mg# (50.2% - 52.1% vs. 53.6% - 72.8%) and compatible trace elements such as Ni (90 - 140 ppm vs. 140 - 550 ppm), Cr (70 - 130 ppm vs. 150 - 930 ppm) and Co (42 - 44 ppm vs. 47% - 68%) than basalts, ankaramite and oceanites from recent Karthala (**Figure 6**). These geochemical characteristics suggest that the magma of ancient Karthala is more evolved than that of recent Karthala. In addition, the basalts of actual Karthala have more variable chemical compositions (SiO_2 = 46.1% - 48.5%; TiO_2 = 1.9% - 2.7%; Al_2O_3 = 10.7% - 14.9%; Na_2O = 2.4% - 3.4%; K_2O = 0.9% - 1.3%; Ni = 70 - 550 ppm; Cr = 30 - 740 ppm; Co = 39 - 68 ppm; La = 27.7 - 40 ppm; Y = 18.9 - 27.3 ppm and Yb = 1.5 - 2.3 ppm) that overlap those of ancient and recent Karthala (**Figure 6**). Finally, the chemical compositions of Karthala massif rocks (ancient, recent and actual) show with Mg# ($Mg\# = ((MgO/40)/(MgO/40) + (Fe_2O_3/72)) \times 100$) used as an index of magmatic differentiation good negative correlations for SiO_2, TiO_2, Al_2O_3, Na_2O, K_2O, P_2O_5, La, Y and Yb and good positive correlations for Ni, Cr and Co (**Figure 6**). These geochemical trends are consistent with the successive crystallization of olivines, pyroxenes, plagioclases and ferrotitanium oxides.

4.2.2. REE and Other Trace Elements

Early Karthala alkaline basalts with ΣREE ranging between 960 and 1011 ppm have highly enriched LREEs of 216 to 236 times chondrites and highly depleted HREEs of 12.6 to 12.9 times chondrites with highly fractionated spectra (LaN/YbN = 16.1 - 17.2) and very weak negative europium anomalies (Eu/Eu* =

Table 1. Geochemical analyses of major and trace elements in basalts, oceanites and ankaramites from the Karthala massif, Abbreviations: Bnvp: Porphyritic non-vesicular basalt; Bvp: Porphyritic vesicular basalt, An: Ankaramite, Oc: Oceanite.

Massif	Old karthala		recent Karthala					actual Karthala					
sample	A19	A22	A18	A20	A21	A5	A11	A2	A15	A16	A17	A12	A14
Lithology	Bvp	Bnvp	Bvp	Bnvp	An	Oc	Oc	Bvp	Bvp	Bvp	Bvp	Bnvp	Bnvp
SiO_2	48.66	48.05	46.71	47.9	46.45	46.4	46.79	48.51	47.78	48.08	46.14	46.96	48.41
Al_2O_3	14.69	14.15	11.49	14.53	9.56	11.57	11.99	14.68	12.92	14.33	10.69	14.47	14.93
Fe_2O_3(T)	12.75	12.58	13.22	12.56	12.16	12.34	12.81	13.19	12.12	12.94	12.9	13.37	13.04
MnO	0.179	0.178	0.177	0.177	0.177	0.18	0.183	0.185	0.173	0.186	0.184	0.189	0.182
MgO	6.44	6.85	12.71	7.26	16.27	12.41	12.35	6.07	8.13	6.97	15.87	6.85	5.38
CaO	11.61	11.26	10.88	11.24	11.27	11.01	11.14	11.62	13.48	11.34	9.38	11.31	10.62
Na_2O	3.1	3.1	2.57	3.09	1.84	2.34	2.62	3.24	2.67	3.17	2.44	3.2	3.38
K_2O	1.17	1.17	0.98	1.13	0.61	1.01	0.96	1.3	0.93	1.26	0.98	1.33	1.27
TiO_2	2.587	2.597	2.278	2.499	1.638	2.034	2.083	2.619	2.161	2.515	1.932	2.627	2.72
P_2O_5	0.36	0.38	0.37	0.36	0.22	0.3	0.29	0.39	0.31	0.37	0.29	0.42	0.41
LOI	0.71	0.49	0.44	0.16	0.54	0.37	0.71	0.91	0.66	0.74	0.67	0.59	0.67
Total	100.84	99.83	100.95	100.59	99.66	99.96	100.51	100.89	100.01	100.42	100.14	100.14	99.67
Mg#	50.23	52.11	65.76	53.59	72.78	66.77	65.83	47.9	57.27	51.84	71.08	50.58	45.19
Ni	90	140	360	140	550	390	380	80	150	130	550	130	70
Cr	70	130	640	150	930	550	550	50	480	130	740	150	30
Co	42	44	54	47	68	59	59	45	44	46	68	46	39
Sc	31	28	31	27	37	31	32	28	39	29	28	25	23
Cs	0.2	0.2	0.2	0.2	0.1	0.2	0.2	0.2	0.2	0.2	0.2	0.3	0.3
Rb	24	25	21	25	13	21	20	27	21	26	21	30	28
Ba	330	352	291	347	202	289	288	370	289	360	284	393	380
Th	3.84	4.17	3.34	4.02	2.23	3.23	3.25	4.05	3.36	3.87	3.07	4.65	4.45
U	0.98	1.03	0.77	0.98	0.55	0.84	0.79	1.02	0.85	0.95	0.75	1.18	1.09
v	290	284	240	280	225	252	259	297	276	291	226	295	286
Nb	40.9	45.5	36.8	41.1	24.8	34	34.6	44.5	35.2	43.2	32.8	48.6	45.9
Ta	2.56	2.89	2.17	2.68	1.53	2.16	2.19	2.87	2.26	2.76	2.05	3.06	2.9
La	34.1	37.3	29.5	34.7	20.4	29.8	29.8	37	29.1	35.2	27.7	40	38
Ce	67.7	72.5	59.3	67.6	40.6	57.7	58.4	70.8	56	69.7	53.6	78.1	72.2
Pb	3	4	4	4	4	9	4	4	4	4	4	4	9
Pr	7.98	8.53	7.06	7.94	4.54	6.66	6.89	8.45	6.52	8.08	6.3	8.78	8.55
Sr	501	515	422	544	308	436	456	526	420	512	392	553	532
Nd	33.2	34.5	27.5	31.8	19.8	27.6	27.8	34.3	28.2	33.4	27	35.9	34.5
Zr	189	196	166	183	110	150	152	199	150	194	150	201	199
Sm	7.13	7.28	5.81	6.67	4.28	5.71	5.81	7.35	5.96	6.64	5.18	7.53	7.32

Continued

Eu	2.11	2.2	1.85	2.13	1.39	1.74	1.85	2.26	1.85	2.1	1.66	2.31	2.18
Gd	6.39	6.67	5.46	6.09	3.9	4.79	4.99	6.6	5.13	6.4	4.7	6.67	6.57
Dy	5.29	5.16	4.37	4.77	3.4	4.13	4.06	5.37	4.65	5.02	3.68	5.59	5.71
Ho	0.98	0.97	0.78	0.91	0.62	0.79	0.75	0.99	0.85	0.95	0.69	1	1.01
Er	2.52	2.49	2.02	2.37	1.65	2.01	2.02	2.58	2.21	2.52	1.86	2.63	2.67
Y	26.1	25.8	21	23.9	16.5	20.4	20.9	25.5	22.2	24.8	18.9	26.1	27.3
Yb	2	2.04	1.59	1.83	1.28	1.6	1.63	1.97	1.71	1.81	1.51	1.99	2.31
Lu	0.301	0.309	0.231	0.279	0.188	0.237	0.25	0.319	0.254	0.275	0.234	0.301	0.345
Sn	1	1	1	1	1	<1	1	1	1	1	<1	1	1
Sb	<0.2	<0.2	<0.2	<0.2	<0.2	<0.2	<0.2	<0.2	<0.2	<0.2	<0.2	<0.2	<0.2
Tb	0.99	1.02	0.81	0.91	0.65	0.78	0.77	0.99	0.82	0.96	0.71	1.03	1.05
W	<0.5	1.1	<0.5	0.6	<0.5	<0.5	0.5	0.7	<0.5	0.8	<0.5	0.7	0.8
Ta	2.56	2.89	2.17	2.68	1.53	2.16	2.19	2.87	2.26	2.73	2.05	3.06	2.9
Mo	<2	2	<2	<2	<2	<2	<2	2	<2	2	<2	2	2
Hf	4.6	5.1	4	4.3	2.8	3.8	3.8	5.1	3.9	4.8	3.7	4.7	4.6
ΣREE	960	1011	816	938	581	799	809	1006	808	961	749	1061	1026
La_N/Yb_N	16.08	17.24	17.50	17.88	15.03	17.56	17.24	17.71	16.05	18.34	17.30	18.95	15.51
La_N/Sm_N	3.42	3.66	3.63	3.72	3.41	3.73	3.67	3.60	3.49	3.79	3.82	3.80	3.71
Gd_N/Yb_N	3.05	3.12	3.28	3.18	2.91	2.86	2.92	3.20	2.86	3.38	2.97	3.20	2.72
La_N/Nd_N	2.24	2.35	2.34	2.38	2.24	2.35	2.33	2.35	2.25	2.29	2.23	2.43	2.40
Sm_N/Gd_N	1.54	1.51	1.47	1.51	1.51	1.65	1.61	1.54	1.60	1.43	1.52	1.56	1.54
Dy_N/Lu_N	2.09	1.99	2.25	2.03	2.15	2.07	1.93	2	2.18	2.17	1.87	2.21	1.97
Eu/Eu*	0.83	0.84	0.87	0.88	0.90	0.87	0.90	0.86	0.88	0.86	0.89	0.86	0.83

0.83 - 0.84) (Figure 7(a)). Alkaline basalts from recent Karthala (ΣREE = 816 - 938 ppm) also show very marked REE enrichment and fractionation (187 to 220 times chondrites in LREE and LaN/YbN = 17.5 - 17.9) with similarly low europium anomalies (Eu/Eu* = 0.87 - 0.88) (Figure 7(a)). It should be noted, however, that recent Karthala alkaline basalts are less enriched in REE, with slightly steeper spectra and less pronounced negative europium anomalies than ancient Karthala alkaline basalts (Figure 7(a)). Recent Karthala ankaramite (ΣREE = 581 ppm) shows a highly fractionated REE spectrum marked by a strong LREE enrichment of 129 times the chondrites and a clear HREE depletion of 8 times the chondrites with a very steep spectrum (LaN/YbN = 15) and a very weak negative europium anomaly (Eu/Eu* = 0.9) (Figure 7(a)). Recent Karthala oceanites (ΣREE = 799 - 809 ppm) also show very marked enrichment (189 times chondrites in LREE) and fractionation of REE spectra (LaN/YbN = 17.2 - 17.6) and very slight negative europium anomalies (Eu/Eu* = 0.87 - 0.9) (Figure 7(a)). Compared with the alkaline basalts and ankaramite of recent Karthala, these oceanites have REEs

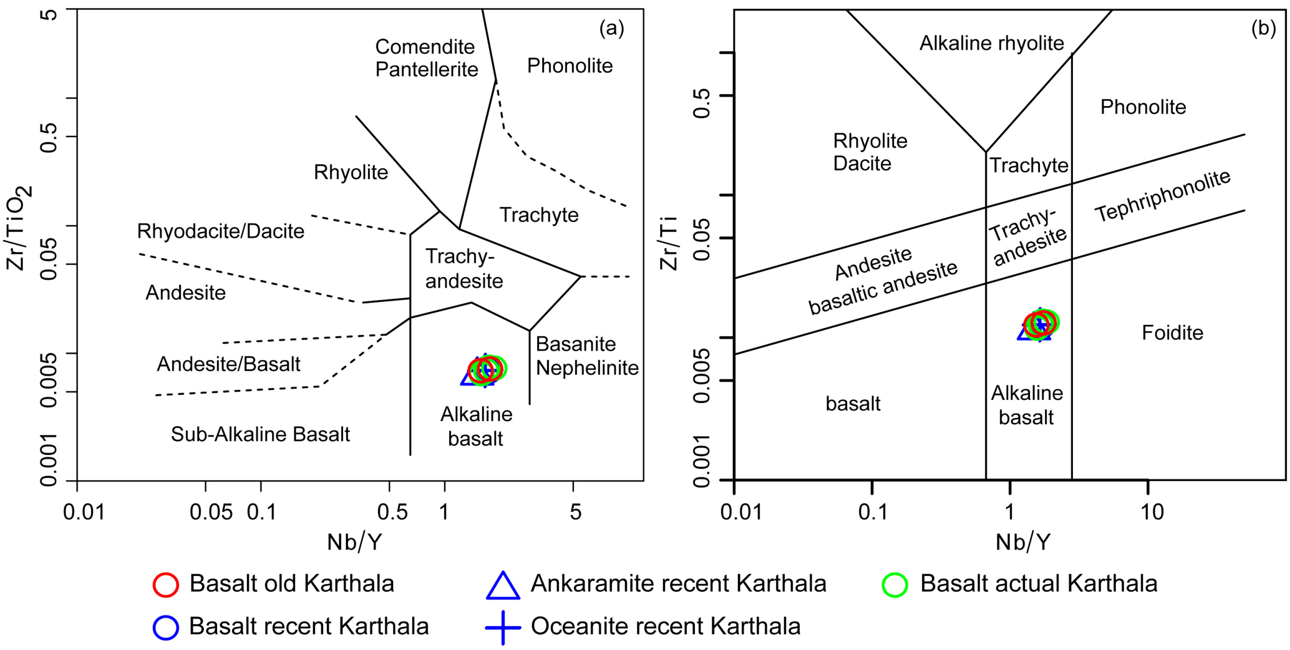

Figure 5. Classification diagrams: (a) Zr/TiO_2 vs Nb/Y from [22] and (b) Zr/Ti vs Nb/Y from [22] modified by [23] showing the alkaline nature of Karthala massif rocks.

intermediate between the two (**Figure 7(a)**). Finally, alkaline basalts from actual Karthala (ΣREE = 749 - 1061 ppm) are slightly more enriched in REE (compared with chondrites 175 to 253 times in LREE and 10 to 14 times in HREE) with spectral fractionation (LaN/YbN = 15.5 - 19) and negative europium anomalies (Eu/Eu* = 0.83 - 0.89) similar to alkaline basalts from ancient and recent Karthala (**Figure 7(a)**).

On the expanded incompatible trace element diagrams normalized to the primitive mantle (**Figure 7(b)**), all samples from ancient, recent and actual Karthala show positive anomalies in Rb, Ba, Ta, Nb and Nd, and negative anomalies in Th, U, Sr and Zr. Pb, on the other hand, shows negative anomalies, with the exception of three samples with positive anomalies (samples: océanite A5 from recent Karthala; ankaramite A21 from recent Karthala and alkaline basalt A14 from actual Karthala).

4.2.3. Nature and Depth of Magmatic Source

In this section, we will use all the samples from the Karthala massif, which are supposed to be representative of magmatic liquids. In the Sm/Yb (ppm) vs. La/Yb (ppm) diagram by [24] (**Figure 8(a)**), Karthala massif lavas lie in the enriched mantle domain and correlate perfectly with asthenospheric mantle melting curves in garnet lherzolite facies. This result is confirmed by the TiO_2/Yb (ppm) versus Nb/Yb (ppm) diagram [25] (**Figure 8(b)**) proposed for estimating the source depth of lavas from oceanic domains not influenced by subduction. In the latter diagram, which confirms the alkaline nature of the rocks, we observe that all lavas lie within the garnet stability field, suggesting that the source of the magma would be very deep garnet lherzolite. The result is also consistent with the very strong

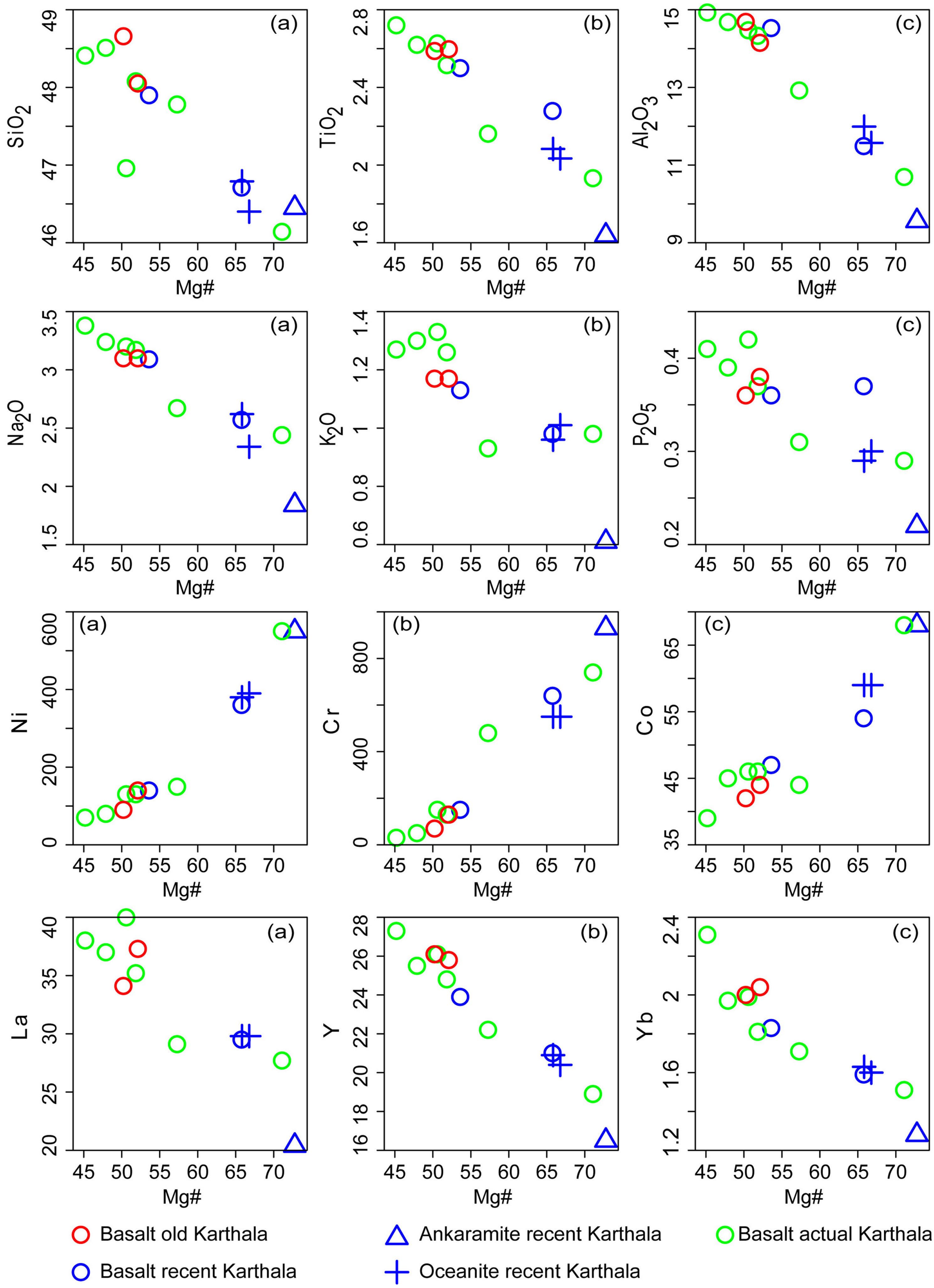

Figure 6. Harker diagrams showing variations in the chemical composition of rocks in the Karthala massif.

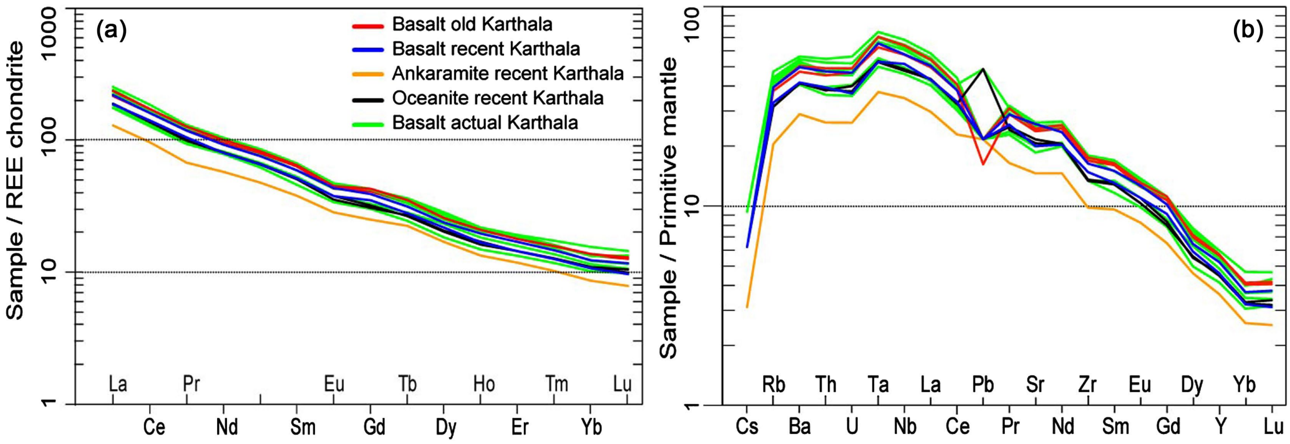

Figure 7. Diagrams: (a) illustrating the REE spectra normalized to the NWA974 chondrites (Barrat *et al*., 2014) and (b) showing the expanded spectra of incompatible elements normalized to the primitive mantle (Sun and McDonough, 1989) of the rocks of the Karthala massif.

depletion of HREEs. However, the heterogeneity of the chemical composition of the magmas that generated the alkaline rocks of ancient, recent and actual Karthala can be explained by a single mantle source, but resulting either from variable rates of partial melting, or from the recycling of subducted oceanic crust residues into the deep mantle [26]. The variable degree of partial melting has been shown to be a function of the LREE/HREE ratio, which can be >1 or <1. Thus, a low partial melting rate gives a LREE/HREE ratio >1, while a high partial melting rate gives a LREE/HREE ratio <1. All the samples from the Karthala massif (ancient, recent and actual) have LREE/HREE (La/Lu) ratios >1. This implies a low partial melting rate for the magmas from which these rocks originate, and this result was confirmed by the Sm/Yb (ppm) vs La/Yb (ppm) diagram [24] (**Figure 8(a)**), which places the rocks from the Karthala massif between 1% and 0.1% partial melting rate. However, the almost identical LREE/HREE ratios between ancient, recent and actual Karthala rocks do not reflect variations in partial melting rates. The differences in chemical composition between ancient, recent and present-day Karthala alkaline rocks are therefore likely to have resulted from the recycling of subducted oceanic crustal residues into the deep mantle, and the interpretation lies in the presence of positive Nb and negative Pb anomalies in the alkaline rocks of the Karthala massif. The distance of the Comoros Islands from the mid-ocean ridge suggests an interaction between the mantle plume and a thick oceanic lithosphere, which could also explain the variability in the chemical composition of the Karthala basalts [27].

4.2.4. Geodynamic Context

To constrain geodynamic environments, we have used discrimination diagrams involving immobile elements such as HFSEs and REEs. Examples include the TiO_2/Yb (ppm) versus Nb/Yb (ppm) (**Figure 8(b)**) or Th/Yb versus Nb/Yb diagrams by [25] (**Figure 9(a)**) and the Nb/Y versus Zr/Y diagram by [28] (**Figure 9(b)**), where the Karthala Massif lavas are located in the Ocean Island Basalt (OIB) field. Furthermore, in [28] diagram (**Figure 9(b)**), all samples from the Karthala massif lie above the ΔNb line, indicating that the source is related to a mantle plume from the enriched lower mantle and the rocks were emplaced at a hot-spot. The oceanic island context (OIB) for the alkaline rocks of the Karthala massif is also in agreement with the highly enriched LREE spectra and the positive Nb and Ta and negative Pb anomalies (with the exception of three samples).

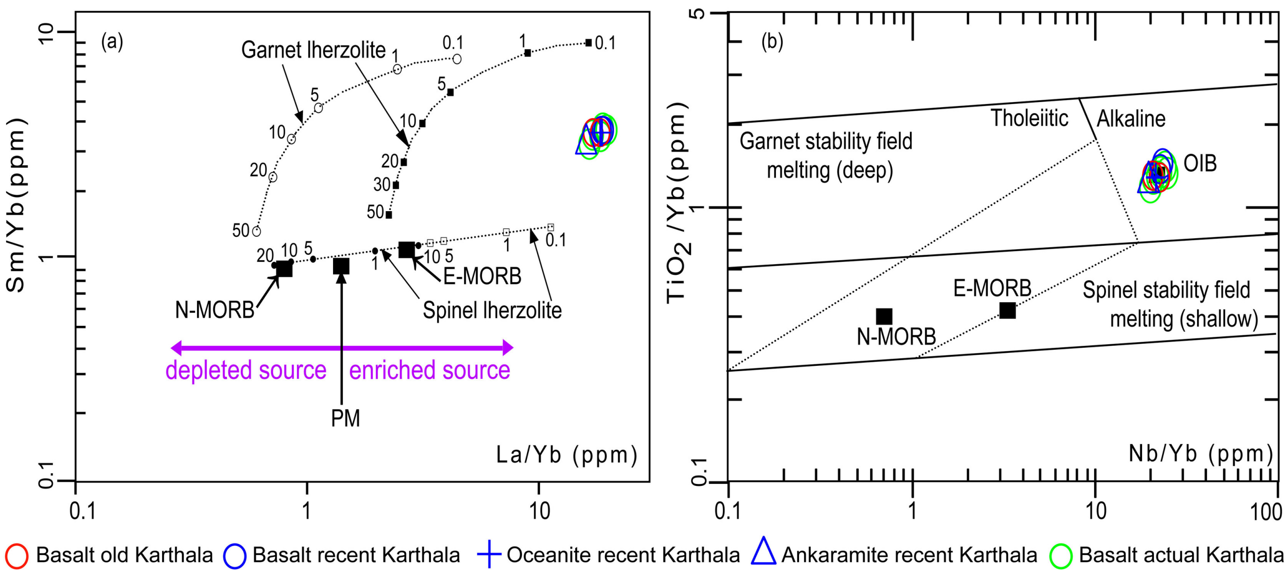

Figure 8. Diagrams: (a) Sm/Yb (ppm) vs La/Yb (ppm) [24] and (b) TiO_2/Yb (ppm) vs Nb/Yb (ppm) [25] showing the nature and depth of the source of the Karthala massif magmas. PM = Primitive Mantle; N-MORB = Normal Mid-Ocean Ridge Basalt; E-MORB = Enriched Mid-Ocean Ridge Basalt; OIB = Ocean Island Basalt. Data from [21].

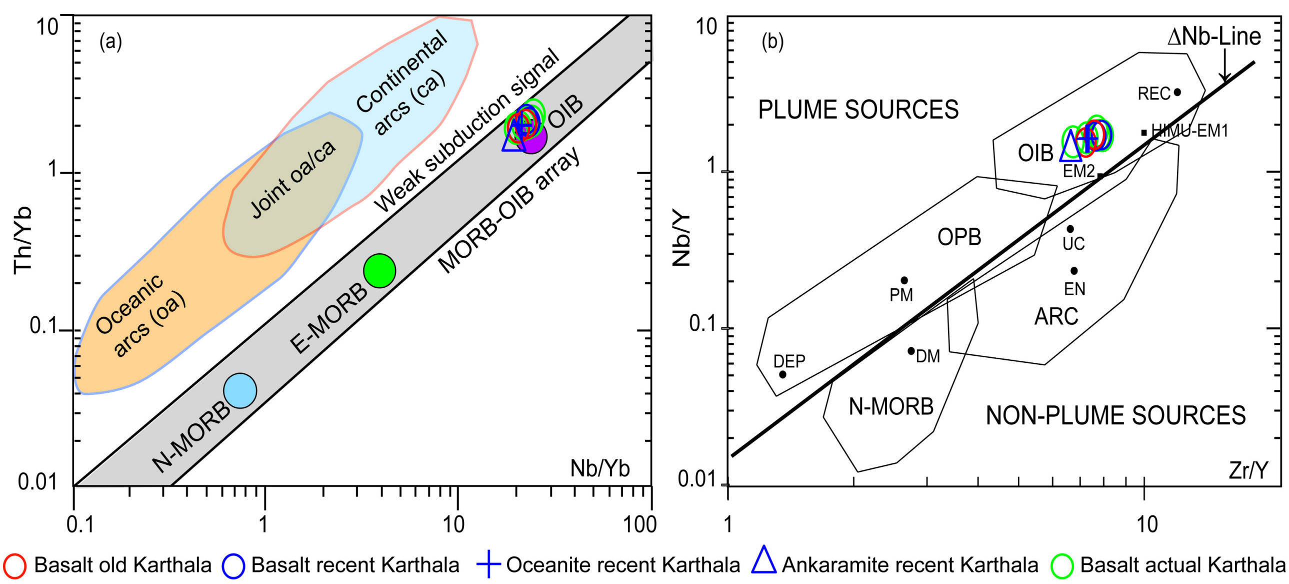

Figure 9. Diagrams: (a) Th/Yb vs Nb/Yb from [25] and (b) Nb/Y vs Zr/Y from [28] showing the compositional ranges of the various oceanic lavas in which the Karthala massif lavas are reported. ARC: arc related basalts; N-MORB: Normal mid ocean ridge basalt; OIB: oceanic island basalt. Hypothetical mantle sources: DM = shallow depleted mantle; EN = enriched component; PM = primitive mantle; REC = recycling component; UC = upper continental crust; DEP = depleted plume component; HIMU = high (U/Pb) source; EM1 and EM2 = enriched mantle sources (modified after [28] and [29].

5. Discussion

The Karthala massif, which covers two-thirds of Grande Comore Island, is composed mainly of vesicular and non-vesicular massive basalt flows, oceanites, ankaramite and pahoehoe and aa-type lavas.

Petrographic studies of the massive basalts, oceanites and ankaramites of the Karthala massif show variable textures ranging from microlitic porphyry to microlitic vacuolar porphyry, and successive crystallization of opaque minerals, olivines, clinopyroxenes, orthopyroxenes and plagioclases. This crystallization order is comparable to that of the basalts and oceanites of Reunion Island [30]-[32], the basalts of Sainte Helene [33] and the basalts of the Karthala massif [15], marked by the early crystallization of spinels or chromites followed by olivines, clinopyroxenes and plagioclases. It should be noted, however, that the basalts in this study and in Réunion are distinguished by the presence of orthopyroxenes, which crystallize after clinopyroxenes. On the other hand, this crystallization order is different from that of the basalts of the Bangaani sector (Karthala massif), marked by the early crystallization of olivines followed by opaque minerals, clinopyroxenes and plagioclases [34] or the basalts of the Azores, Tristan da Cunha and Gough [35]: and Icelandic basalts [36], where opaque minerals crystallized last after olivines, clinopyroxenes and plagioclases in succession.

The geochemical study confirms the alkaline nature of the basalts of the Karthala massif and the non-primary nature of the magmas that produced the rocks of ancient, recent and actual Karthala. This result confirms that of [1], who showed that the Karthala lavas are non-primary due to their low Mg# values of between 0.52 and 0.54, their low Ni contents (115 and 122 ppm) and their low Ni/MgO ratios of between 16.9 and 18.1. Moreover, this geochemical study also indicates a single source and variability in the chemical composition of the magmas that generate the rocks of ancient, recent and present-day Karthala; variability probably due either to different partial melting rates or to the great thickness of the oceanic lithosphere [27]. This latter result contradicts that of [37], who had suggested that the variability in the chemical composition of the basalts of the Karthala massif is consistent with the mixing of plume and lithosphere-derived melts. In addition, the magmatic source of the Karthala massif rocks is a very deep garnet lherzolite located in the lower mantle. The magmas would be generated from mantle plumes and then spread by a hot spot. This result is similar to that of [38], who suggested that the source of the Karthala massif rocks lies at greater depth and that the garnet content of the residue should be greater. On the other hand, it contradicts that of [1], who showed that the basalts of the Karthala massif originated from a slightly larger partial melting of garnet or spinel-bearing lherzolite at slightly shallower depths, and that of [16], which indicates an identical degree of partial melting affecting a single source where phlogopite and garnet are more or less residual.

6. Conclusions

The formations of the Karthala massif consist of massive vesicular and non-vesicular basalts, oceanites, ankaramites and pahoehoe and aa-type flow effusions up to several kilometers in extent.

Petrographic studies of Karthala basalts, oceanites and ankaramites reveal porphyritic and vacuolated porphyritic microlitic textures marked by successive crystallization of opaque minerals, olivines, clinopyroxenes, orthopyroxenes and plagioclases in little or no mesostasis. It should be noted, however, that this is the first time that an orthopyroxene mineral has been identified by this study in the Karthala massif.

The geochemical study confirms the alkaline affinity of the rocks and shows a very strong enrichment in LREE and a clear depletion in HREE marked by very steep spectra and positive anomalies in Nb and Ta and negative in Pb. These geochemical characteristics are compatible with a deep, enriched mantle source of garnet lherzolite type located in the lower mantle. However, the magmas that give rise to the alkaline rocks of ancient, recent and actual Karthala are thought to have different chemical compositions and to have risen as mantle plumes in a hot-spot intraplate context to generate oceanic island basalts (OIBs).

Acknowledgements

We would like to thank the National Center for Scientific Research and Documentation (CNDRS) of the Comoros for allowing us to carry out a field campaign in the Karthala summit caldera. Our thanks also go to Mr. Chafik Bafakih, former head of the Karthala Volcanology Observatory (OVK), who always had a positive view of our work.

We would also like to thank Mr. Baba Sarr and Mrs. Safiétou Senghor of the petrology and structural laboratory of the Fundamental Institute of Black Africa (IFAN) at the Cheikh Anta Diop University in Dakar, Senegal, for authorizing and assisting us during microscopic observations and the production of microphotographs.

Conflicts of Interest

The authors declare no conflicts of interest regarding the publication of this paper.

References

[1] Spāth, A., Roex, A.P.L. and Duncan, R.A. (1996) The Geochemistry of Lavas from the Gomores Archipelago, Western Indian Ocean: Petrogenesis and Mantle Source Region Characteristics. *Journal of Petrology*, **37**, 961-991. https://doi.org/10.1093/petrology/37.4.961

[2] Class, C. and Goldstein, S.L. (1997) Plume-Lithosphere Interactions in the Ocean Basins: Constraints from the Source Mineralogy. *Earth and Planetary Science Letters*, **150**, 245-260. https://doi.org/10.1016/s0012-821x(97)00089-7

[3] Class, C., Goldstein, S.L., Altherr, R. and Bachelery, P. (1998) The Process of Plume-Lithosphere Interactions in the Ocean Basins—The Case of Grande Comore. *Journal of Petrology*, **39**, 881-903. https://doi.org/10.1093/petroj/39.5.881

[4] Claude-Ivanaj, C., Bourdon, B. and Allègre, C.J. (1998) Ra–Th–Sr Isotope Systemat-

ics in Grande Comore Island: A Case Study of Plume-Lithosphere Interaction. *Earth and Planetary Science Letters*, **164**, 99-117. https://doi.org/10.1016/s0012-821x(98)00195-2

[5] Deniel, C. (1998) Geochemical and Isotopic (Sr, Nd, Pb) Evidence for Plume-Lithosphere Interactions in the Genesis of Grande Comore Magmas (Indian Ocean). *Chemical Geology*, **144**, 281-303. https://doi.org/10.1016/s0009-2541(97)00139-3

[6] Famin, V., Michon, L. and Bourhane, A. (2020) The Comoros Archipelago: A Right-Lateral Transform Boundary between the Somalia and Lwandle Plates. *Tectonophysics*, **789**, Article 228539. https://doi.org/10.1016/j.tecto.2020.228539

[7] Nougier, J., Cantagrel, J.M. and Karche, J.P. (1986) The Comores Archipelago in the Western Indian Ocean: Volcanology, Geochronology and Geodynamic Setting. *Journal of African Earth Sciences* (1983), **5**, 135-145. https://doi.org/10.1016/0899-5362(86)90003-5

[8] Michon, L., Ferrazzini, V. and Di Muro, A. (2015) Magma Paths at Piton de la Fournaise Volcano. In: Bachelery, P., Lenat, J.F., Di Muro, A. and Michon, L., Eds., *Active Volcanoes of the World*, Springer, 91-106. https://doi.org/10.1007/978-3-642-31395-0_7

[9] Dixey, F. (1956) Geol, and Min. Ressource Sup. Ser.71.

[10] Hajash, A. and Armstrong, R.L. (1972) Paleomagnetic and Radiometric Evidence for the Age of the Comores Islands, West Central Indian Ocean. *Earth and Planetary Science Letters*, **16**, 231-236. https://doi.org/10.1016/0012-821x(72)90195-1

[11] Flower, M.F.J. and Strong, D.F. (1969) The Significance of Sandstone Inclusions in Lavas of the Comores Archipelago. *Earth and Planetary Science Letters*, **7**, 47-50. https://doi.org/10.1016/0012-821x(69)90010-7

[12] Coffin, M.F. and Rabinowitz, P.D. (1987) Reconstruction of Madagascar and Africa: Evidence from the Davie Fracture Zone and Western Somali Basin. *Journal of Geophysical Research*: *Solid Earth*, **92**, 9385-9406. https://doi.org/10.1029/jb092ib09p09385

[13] Battistini, R. (1996) Paléogéographie et variété des milieux naturels à Madagascar et dans les voisines: Quelques données de base pour l'étude biogéographique de la (reGion Malgache). Editions de I'orstom, 1-17.

[14] Emerick, C.M. and Duncan, R.A. (1982) Age Progressive Volcanism in the Comores Archipelago, Western Indian Ocean and Implications for Somali Plate Tectonics. *Earth and Planetary Science Letters*, **60**, 415-428. https://doi.org/10.1016/0012-821x(82)90077-2

[15] Desgrolard, F. (1996) Pétrologie des laves d'un volcan intraplaque océanique: Le Karthala, île de la Grande-Comore (R.F.I. des Comores). Université Joseph-Fourier-Grenoble I, 176.

[16] Malood, J.A., Mougenot, D., Raillard, S. and Maillard, A. (1991) Nouvelles contraintes sur la cinétique de Madagascar: Les structures de la chaine de Davie. *Comptes rendus de l'Académie des Sciences*, **312**, 1639-1646.

[17] Debeuf, D. (2004) Etude de l'évolution volcano-structurale et magmatique de Mayotte (Archipel des Comores, Océan Indien): Approches structurale, pétrographique, géochimique et géochronologique. Thèse, Université de La Réunion, 277.

[18] Bachelery, P. and Coudray, J. (1993) Carte volcano-téctonique de la'Grande Comore Ngazidja au 1/50000 avec notice explicative. Ed. Mission Française de coopération aux Comores.

[19] Bachèlery, P., Morin, J., Villeneuve, N., Soulé, H., Nassor, H. and Radadi Ali, H.

(2015) Structure and Eruptive History of Karthala Volcano. In: Bachèlery, P., Lénat, J.-F., Di Muro, A. and Michon, L., Eds., *Active volcanoes of the Southwest Indian Ocean*: *Piton de la Fournaise and Karthala*. *Active volcanoes of the world*, Springer, 345-366. https://doi.org/10.1007/978-3-642-31395-0

[20] Barrat, J.A., Zanda, B., Jambon, A. and Bollinger, C. (2014) The Lithophile Trace Elements in Enstatite Chondrites. *Geochimica et Cosmochimica Acta*, **128**, 71-94. https://doi.org/10.1016/j.gca.2013.11.042

[21] Sun, S.-S. and McDonough, W.F. (1989) Chemical and Isotopic Systematics of Oceanic Basalts: Implications for Mantle Composition and Processes. *Geological Society*, *London*, *Special Publications*, **42**, 313-345. https://doi.org/10.1144/gsl.sp.1989.042.01.19

[22] Winchester, J.A. and Floyd, P.A. (1977) Geochemical Discrimination of Different Magma Series and Their Differentiation Products Using Immobile Elements. *Chemical Geology*, **20**, 325-343. https://doi.org/10.1016/0009-2541(77)90057-2

[23] Pearce, J.A. (1996) A User's Guide to Basalt Discrimination Diagrams. In: Wyman, D.A., ed., *Trace Element Geochemistry of Volcanic Rocks*: *Applications for Massive Sulphide Exploration*: *Geological Association of Canada*, *Short Course Notes*, Vol. 12, St. John's, 79-113.

[24] Aldanmaz, E., Pearce, J.A., Thirlwall, M.F. and Mitchell, J.G. (2000) Petrogenetic Evolution of Late Cenozoic, Post-Collision Volcanism in Western Anatolia, Turkey. *Journal of Volcanology and Geothermal Research*, **102**, 67-95. https://doi.org/10.1016/s0377-0273(00)00182-7

[25] Pearce, J.A. (2008) Geochemical Fingerprinting of Oceanic Basalts with Applications to Ophiolite Classification and the Search for Archean Oceanic Crust. *Lithos*, **100**, 14-48. https://doi.org/10.1016/j.lithos.2007.06.016

[26] Juteau, T. and Maury, M. (2012) La croûte océanique: Pétrologie et dynamique endogène. Livre Publié éDition Vuilert, 579 p.

[27] Jiang, S., Hawkins, R., Hoggard, M.J., Davies, D.R. and Campbell, I.H. (2024) Investigating the Lid Effect on the Generation of Ocean Island Basalts: 1. Geochemical Trends. *Geochemistry*, *Geophysics*, *Geosystems*, **25**, e2023GC011387. https://doi.org/10.1029/2023gc011387

[28] Condie, K.C. (2005) High Field Strength Element Ratios in Archean Basalts: A Window to Evolving Sources of Mantle Plumes? *Lithos*, **79**, 491-504. https://doi.org/10.1016/j.lithos.2004.09.014

[29] Condie, K.C. (2003) Incompatible Element Ratios in Oceanic Basalts and Komatiites: Tracking Deep Mantle Sources and Continental Growth Rates with Time. *Geochemistry*, *Geophysics*, *Geosystems*, **4**, 1-28. https://doi.org/10.1029/2002gc000333

[30] Lénat, J., Boivin, P., Deniel, C., Gillot, P. and Bachèlery, P. (2009) Age and Nature of Deposits on the Submarine Flanks of Piton De La Fournaise (Reunion Island). *Journal of Volcanology and Geothermal Research*, **184**, 199-207. https://doi.org/10.1016/j.jvolgeores.2009.01.013

[31] Boudoire, G., Brugier, Y.-A., Di Muro, A., Wörner, G., Arienzo, I., Metrich, N., *et al.* (2019) Eruptive Activity on the Western Flank of Piton De La Fournaise (La Réunion Island, Indian Ocean): Insights on Magma Transfer, Storage and Evolution at an Oceanic Volcanic Island. *Journal of Petrology*, **60**, 1717-1752. https://doi.org/10.1093/petrology/egz045

[32] Welsch, B. (2010) Signification des Océanites dans le fonctionnement du Piton de la Fournaise, Île de La Réunion. Thèse de l'Université de La Réunion.

[33] Kawabata, H., Hanyu, T., Chang, Q., Kimura, J., Nichols, A.R.L. and Tatsumi, Y. (2011) The Petrology and Geochemistry of St. Helena Alkali Basalts: Evaluation of the Oceanic Crust-Recycling Model for HIMU OIB. *Journal of Petrology*, **52**, 791-838. https://doi.org/10.1093/petrology/egr003

[34] Cissokho, S., Ahamada, A., Ndiaye, A., Yatte, D. and Ngom, P.M. (2023) Contribution to the Petrographic and Geochemical Study of the Karthala Massif Lavas in the Bangaani Area, Grande Comore, Indian Ocean. *Open Journal of Geology*, **13**, 312-336. https://doi.org/10.4236/ojg.2023.135016

[35] White, W.M., Tapia, M.D.M. and Schilling, J.-C. (1979) The Petrology and Geochemistry of the Azores Islands. *Contributions to Mineralogy and Petrology*, **69**, 201-213. https://doi.org/10.1007/bf00372322

[36] Hansen, H. and Grönvold, K. (2000) Plagioclase Ultraphyric Basalts in Iceland: The Mush of the Rift. *Journal of Volcanology and Geothermal Research*, **98**, 1-32. https://doi.org/10.1016/s0377-0273(99)00189-4

[37] Bachèlery, P. and Hémond, C. (2015) Geochemical and Petrological Aspects of Karthala Volcano. In: Bachelery, P., Lenat, J.F., Di Muro, A. and Michon, L., Eds., *Active Volcanoes of the World*, Springer, 367-384. https://doi.org/10.1007/978-3-642-31395-0_23

[38] Bourdon, B., Joron, J., Claude-Ivanaj, C. and Allègre, C.J. (1998) U-Th-Pa-Ra Systematics for the Grande Comore Volcanics: Melting Processes in an Upwelling Plume. *Earth and Planetary Science Letters*, **164**, 119-133. https://doi.org/10.1016/s0012-821x(98)00227-1